Original Article

MOLECULAR METABOLISM

Deletion of *Six3* in post-proliferative neurons produces weakened SCN circadian output, improved metabolic function, and dwarfism in male mice

Jason D. Meadows [1,2], Joseph A. Breuer [1,2], Shanna N. Lavalle [1,2], Michael R. Hirschenberger [3], Meera M. Patel [1], Duong Nguyen [3], Alyssa Kim [4], Jessica Cassin [1], Michael R. Gorman [2,5], David K. Welsh [2,6,7], Pamela L. Mellon [1,2], Hanne M. Hoffmann [1,2,3,*]

ABSTRACT

Objective: The increasing prevalence of obesity makes it important to increase the understanding of the maturation and function of the neuronal integrators and regulators of metabolic function.

Methods: Behavioral, molecular, and physiological analyses of transgenic mice with Sine oculis 3 (*Six3*) deleted in mature neurons using the *Synapsin^{cre} allele.*

Results: Conditional deletion of the homeodomain transcription factor *Six3* in mature neurons causes dwarfism and weakens circadian wheel-running activity rhythms but increases general activity at night, and improves metabolic function, without impacting pubertal onset or fertility in males. The reduced growth in 6-week-old *Six3$^{fl/fl}$:Synapsin^{cre}* (*Six3^{syn}*) males correlates with increased somatostatin (SS) expression in the hypothalamus and reduced growth hormone (GH) in the pituitary. In contrast, 12-week-old *Six3^{syn}* males have increased GH release, despite an increased number of the inhibitory SS neurons in the periventricular nucleus. GH is important in glucose metabolism, muscle function, and bone health. Interestingly, *Six3^{syn}* males have improved glucose tolerance at 7, 12, and 18 weeks of age, which, in adulthood, is associated with increased % lean mass and increased metabolic rates. Further, 12-week-old *Six3^{syn}* males have reduced bone mineralization and a lower bone mineral density, indicating that reduced GH levels during early life cause a long-term reduction in bone mineralization.

Conclusion: Our study points to the novel role of *Six3* in post-proliferative neurons to regulate metabolic function through SS neuron control of GH release.

Keywords Somatostatin; Growth hormone; Metabolism; Circadian rhythm; Suprachiasmatic nucleus; Six homeobox 3

1. INTRODUCTION

Obesity is an increasing problem worldwide, with the World Health Organization estimating 1.9 billion adults were overweight in 2016, and 39 million children under the age of 5 were overweight or obese in 2020 [1]. Overweight and obesity are associated with increased risks of type 2 diabetes [2] and cardiovascular problems [3], among many other negative health outcomes. Although obesity is reversible and preventable through sustained changes in lifestyle, such approaches often fail. It, therefore, remains a priority to identify genes and pharmacological targets that regulate food intake and metabolic function, which are potential novel treatment strategies to help reduce the current worldwide epidemic of obesity.

Food intake and energy expenditure are regulated by the hypothalamus [4–6]. To maintain metabolic homeostasis, peripheral signals are integrated by hypothalamic nuclei, including the arcuate nucleus, periventricular nucleus (PeVN), and paraventricular nucleus (PVN). The function of these brain structures is aligned to the time-of-day and metabolic cues, such as meal hours. Time-of-day information is transmitted to the arcuate nucleus, PeVN, and PVN through direct projections from the suprachiasmatic nucleus (SCN). The SCN receives light information from the eye and translates it into neuronal and

[1]Department of Obstetrics, Gynecology, and Reproductive Sciences and Center for Reproductive Science and Medicine, University of California, San Diego, 9500 Gilman Drive, La Jolla, CA, 92093, USA [2]Center for Circadian Biology, University of California, San Diego, La Jolla, CA, 92093, USA [3]Department of Animal Science and the Reproductive and Developmental Sciences Program, Michigan State University, 766 Service Road, East Lansing, MI, 48824, USA [4]Department of Plant Soil and Microbial Sciences, Michigan State University, and CANR Statistical Consulting Center, Michigan State University, East Lansing, MI, 48824, USA [5]Department of Psychology, University of California, San Diego, La Jolla, CA, 92093, USA [6]Department of Psychiatry, University of California, San Diego, La Jolla, CA, 92093, USA [7]Veterans Affairs San Diego Healthcare System, San Diego, CA, 92161, USA

*Corresponding author. Michigan State University Interdisciplinary Science and Technology Building #3010 766 Service Road, East Lansing, MI 48224, USA. E-mail: hanne@msu.edu (H.M. Hoffmann).

Received September 23, 2021 • Revision received December 17, 2021 • Accepted December 29, 2021 • Available online 31 December 2021

https://doi.org/10.1016/j.molmet.2021.101431

endocrine signals, providing day-length and light information to non-SCN brain areas and peripheral tissues. Disruption of SCN circadian time keeping or molecular clock function can negatively affect metabolic function and is associated with an increased risk of metabolic disease and diabetes [7–11]. Metabolic dysregulation can be induced through genetic approaches such as knock-out (KO) of molecular clock genes, including *Bmal1,* expression of the dominant-negative *ClockΔ19* mutant [5,6], or light-induced circadian disruption. These relationships between metabolic function and circadian rhythms are further evidenced in studies focusing on feeding time, where time-restricted feeding, or eating earlier in the day, reduces weight gain and improves metabolic function [12]. This points to an interesting interaction between the circadian system, feeding, and metabolic status.

In addition to mis-timed light and poor eating patterns as risk factors in the development of overweight and obesity, genetic factors also contribute to the deregulation of metabolic function. Mutations in genes encoding neuropeptides, hormones, and their receptors that regulate hypothalamic function, including the genes encoding for POMC (pro-opiomelanocortin), leptin, and leptin receptor, cause obesity in rodents and humans [4]. A second set of genes pointing to the key role of dysregulated hypothalamic function as a cause of overweight and obesity are mutations in genes coding for transcription factors required for hypothalamic development and function, such as SIM1 [13,14]. A novel candidate gene involved in hypothalamic function is Sine oculis 3 (*Six3*) [15]. SIX3 is a homeodomain transcription factor required for retinal, forebrain, and pituitary development [16–24]. After embryonic development, *Six3* retains a broad expression pattern in the brain [25], where it regulates radial glia maturation into ependymal cells [26], medium spiny neuron plasticity and striatal function [27–29], hypothalamic kisspeptin neuron function [30], as well as SCN function [25]. However, the potential role of *Six3* in metabolism remains unexplored.

Based on the high expression of *Six3* in the developing and adult male hypothalamus, and our previous work showing dysregulated hypothalamic function in female mice with *Six3* deleted in post-proliferative neurons using a *Synapsin*^{cre} allele (*Six3*^{syn} mice), we hypothesize that *Six3*^{syn} males also have dysregulated hypothalamic function and impaired SCN circadian time keeping, which we predict will negatively impact glucose metabolism, increasing fat accumulation, and body weight.

2. MATERIALS AND METHODS

2.1. Mouse breeding

All animal procedures were performed according to the protocols approved by the Institutional Animal Care and Use Committees of University of California San Diego and Michigan State University, and were conducted in accordance with the Guide for the Care and Use of Laboratory Animals (National Research Council, 2011). Mice were maintained on a light/dark cycle of LD [12 h light, 12 h dark; lights on 6 AM (Zeitgeber (ZT) 0) to 6 PM (ZT12)], with ad libitum access to water and chow (Teklad S-2335 Mouse Breeder Irradiated Diet, Envigo). *Per2::LUC* [Tg (Per2-luc)1Jt, JAX#006852]; *Six3*^{flox} [Six3^{tm2Gco}, MGI 3693321] mice [31] were crossed with either *Kiss1*^{Cre} mice [32,33] or *Synapsin*^{cre} [B6.Cg-Tg (Syn1-cre)671Jxm/J, JAX #003966] mice. All Cre^{+} mice were heterozygous for their respective Cre-alleles. Genotyping primer sequences were as follows: Per2F: CAAAGGCACCTCCAACATG, Per2R: AAAGTATTTGCTGGTGTGACTTG; CreF: GCATTACCG GTCGTAGCAACGAGTG, CreR: GAACGCTAGAGCCTGTTTTGCACGTTC; Six3wtF: TTCCCCTCTTTGACTCCTATGGACG, Six3floxF: CGGCCCATGTA CAACGCGTATT, Six3R: CCCCTAGCCTAACCCAAACATTCG; *Six3*^{flox} were on a mixed C57BL/6J/NMRI background [31]. All mice were screened for germline recombination using PCR, and germline recombined mice were eliminated from the study. Mice were euthanized by CO_2 or isoflurane (Vet One, Meridian, ID) anesthesia followed by decapitation.

2.2. PCR to detect flox-allele recombination

To detect *Synapsin*^{cre}-induced *Six3*^{flox} allele recombination, males were euthanized with CO_2 overdose at ZT3-6, and hypothalamus, cortex, pituitary, liver, pancreas, white adipose tissue, brown adipose tissue, testis, and tail were frozen. Genomic DNA was extracted using DNeasy Kit (Qiagen) according to manufacturer's instructions. The following primers were used Six3RecF: CCCCTAGCCTAACCCAAACAT, Six3RecR: TTCCCCTCTTTGACTCCTATG, annealing temperature 59 °C. PCR products were separated on a 2% agarose gel.

2.3. Litter size assessment

For litter size assessment, virgin 8- to 12-week-old *Six3*$^{fl/fl}$ and *Six3*^{syn} males were housed with *Six3*$^{fl/fl}$ females [34,35]. The number of pups per litter was recorded for the first 3 litters, as described previously [34].

2.4. Quantitative real-time PCR

For RT-qPCR, the hypothalamus, pituitary, and liver were collected from males that were euthanized by CO_2 overdose between 10AM (ZT4, 4 h after lights ON) and 1 PM (ZT7), except where otherwise stated. Tissues were snap frozen on dry ice and stored at −80 °C until RNA extraction. Total RNA was extracted using TRIzol (Invitrogen). Genomic DNA was eliminated using the DNA-free kit (Applied Biosystems). cDNA was obtained by reverse transcription of total RNA using an iScript cDNA synthesis kit (Bio-Rad Laboratories). cDNA products were detected using an iQ SYBR Green Supermix (Bio-Rad Laboratories) on a qRT-PCR CFX real-time detection system (Bio-Rad Laboratories). qRT-PCR primers (Supplementary Table 1) were previously published [35–37]. Data were expressed as fold change using the 2-δδCT method by normalizing *Gnrh1* to *Gapdh* [38]. Data represent mean fold change ± SEM from a minimum of three mice for each data point.

2.5. Wheel-running behavior

At age 8–12 weeks, males were single housed in cages containing running wheels with magnets, and wheel revolutions were monitored using magnetic sensors. All cages were contained in a light-tight cabinet with programmable lighting and monitored for temperature and humidity. Food and water were available ad libitum during the entire experiment. Males were housed in polypropylene cages (17.8 × 25.4 × 15.2 cm) containing a metal running wheel (11.4 cm diameter), and locomotor activity rhythms were monitored with a VitalView data collection system (Version 4.2, Minimitter, Bend OR) that integrated in 6 min bins the number of magnetic switch closures triggered by half wheel rotations. Running wheel activity was monitored for 4 weeks on LD (light12h:dark12h), where week 1 was considered as adaptation to a novel environment, and the two weeks prior to constant darkness (DD), were used as control baseline activity in LD. Subsequently, mice were monitored for 4 weeks in DD, with wheel running data analyzed from weeks 2 and 3 in DD. Cage changes were scheduled at 3-week intervals. Wheel-running activity was analyzed using ClockLab Analysis (ActiMetrics) by an experimenter blind to experimental group. Circadian period was estimated by constructing a ClockLab-generated least-squares regression line through a minimum of 13 daily activity onsets. Daily onset and offset of

activities, defined as a period of 5 h of activity following 5 h of inactivity (onset) or a period of 5 h of inactivity following 5 h of activity (offset), were used to calculate the duration of the active phase (alpha). Chi^2 periodograms [39] were generated for periods from 0 to 36 h, with a significance criterion set at 0.001. Any mice that did not exhibit a significant peak between 18 and 36 h were deemed arrhythmic and were not included in analyses, and the maximum amplitude was reported as Qp. Activity profiles were generated for weeks 2–4 in DD using the circadian period (tau) estimated from the chi^2 periodogram for the same time interval. Total daily counts were calculated over 24 h, during habituation, LD, and DD.

2.6. Ex vivo tissue recordings of Per2::LUC expression

For SCN, pituitary, epididymis, and liver explant studies, male Per2::LUC circadian reporter mice were used [40]. Males were sacrificed at ZT3-4 via isoflurane inhalation and cervical dislocation. The pituitary, liver, and brain were removed immediately and placed in ice-cold HBSS for approximately 30–60 min. Using a Vibratome (Leica), coronal brain sections of 300 μm were collected, and the SCN was dissected from the slices in ∼2 × 2 mm squares. An SCN, ∼3 × 2 mm liver section, one epididymis, or one pituitary was placed individually on a 30 mm MilliCell membrane (Millipore-Sigma) in a 35 mm cell culture dish containing 1 mL Neurobasal-A Medium (Gibco) with 1% Glutamax (Gibco), B27 supplement (2%; 12,349–015, Gibco), and 1 mM luciferin (BD Biosciences). The lid was sealed to the plate using vacuum grease to ensure an air-tight seal. Plated tissues were loaded into a LumiCycle luminometer (Actimetrics) inside a 35 °C non-humidified incubator at ZT6-6.5, and recordings were started. The bioluminescence was counted for 70 s every 10 min for 6 days (day 1 - day 7 of recording time). Per2:LUC rhythm data were analyzed using LumiCycle Analysis software (Actimetrics) by an experimenter blind to experimental group. Data were detrended by subtraction of the 24 h running average, smoothed with a 2 h running average, and fitted to a damped sine wave (LM Fit, damped). Period was defined as the time in hours between the peaks of the fitted curve. Amplitude was defined as the amplitude of the fitted sine wave [41].

2.7. Dual energy X-ray absorptiometry (DEXA)

Body composition was determined in 12-week-old *Six3*$^{fl/fl}$ and *Six3*^{syn} males by DEXA. Mice were fasted for 4–6 h and then anesthetized (ketamine 100 mg/kg, xylazine 10 mg/kg). Body weight (BW) was measured, and lean muscle mass and fat mass were determined by scanning with a GE Lunar Pixi Densitometer Machine (n = 6 group).

2.8. Weekly growth analyses

Group housed males were weighed once weekly from 3 to 12 weeks of age. Length measurements were done on isoflurane anesthetized males using a caliper. The measurements were taken from the tip of the nose to the base of the tail in 3-, 4-, 6-, 8-, 12-, and 16-week-old males.

2.9. Hormone assays and glucose tolerance tests (GTT)

GTTs were performed in adult *Six3*$^{fl/fl}$ and *Six3*^{syn} male mice on a standard chow diet at 7-, 12-, and 18-weeks of age. Mice were fasted for 6 h before GTT with free access to water. Blood glucose was then measured using a handheld glucometer (One Touch UltraMini, LifeScan, Inc.) just before IP glucose injection (time 0; 2 g/kg BW in saline) and subsequently at 15, 30, 45, 60, 90, and 120 min post-administration using 1 g/kg BW glucose in saline. For all other serum hormone analyses, mice were euthanized by isoflurane overdose between ZT4 to ZT7 and blood collected from the abdominal aorta. Blood was allowed to clot for 1 h at RT, then centrifuged (RT, 15 min, 2600 *g*), and serum stored at −20 °C before Luminex analysis for GH, LH, and FSH on MILLIPLEX MAP Mouse Pituitary Magnetic Bead Panel (Millipore Sigma #MPTMAG-49k). Coefficients of variance (CVs) were based on the variance of samples in the standard curve run in duplicate or triplicate. Lower detection limits: LH = 5.6 pg/mL, CV < 15%; FSH = 25.3 pg/mL, CV < 15% GH = 4.88 pg/mL, GH < 10%. Samples were run in singlets.

2.10. Metabolic and locomotor analyses

Indirect calorimetry was performed on 18- to 21-week-old *Six3*^{syn} males on a standard chow diet using a 12-cage equal flow CLAMS calorimeter system (Columbus Instruments) coupled with photosensors to detect movement. Each cage has internal dimensions of: width (4 cm) x depth (20 cm) x height (13 cm). Males were habituated to the metabolic cages (single-housed) for 2 days prior to data acquisition (n = 6/genotype). O_2 consumption (VO2) and CO_2 production (VCO2) were measured every 12 min in each cage. Respiratory exchange ratio (RER) was calculated as the quotient of VCO2/VO2. Locomotor activity was measured in 1 min intervals by photosensors, with the bottom row measuring horizontal movement (total = total number of photobeams broken; ambulatory = number of consecutive beams broken to exclude non-ambulatory movements like grooming) and the upper row measuring vertical movement (includes rearing, reaching the drinking tube, walking on top of the food hopper). In addition, feeding was measured in 12 min intervals and calculated for hourly feeding. Cage tops were equipped with infrared sensors (TSE InfraMot; TSE Systems) to detect body-heat image and its spatial (3 dimensional) displacement over time to assess general locomotor activity, measured as arbitrary 'InfraMo-units'. Owing to high fluctuations of the respiratory rate readings, CO_2 and O_2 records from each mouse were subjected to the filtering process. The median and standard error were calculated for every 2.5-hour interval (i.e., 12 observations), and the observations within the range of median ± standard error were selected and used for further analysis. There was a total of 306 raw observations of O_2 and CO_2 per cage (mouse), and on average 210 observations were remaining after the filtering process. To fit the sinusoidal curve, each filtered dataset was then fitted with equation $Y = A \sin(B \cdot t + C) + D$ by using optimization functions embedded in the SciPy package in Python 3.6 (Python Software Foundation). Model parameter A indicates the amplitude, B indicates the frequency, C indicates the phase, and D indicates the mean. From the frequency and phase, the time for the VCO2 or VO2 to reach maximum (T_{max}) was calculated. T_{max} was adjusted to have a range between 12 and 36 h after the onset of the start of data collection. The average R^2 values of the curves were 0.43 and 0.45 for O_2 and CO_2 datasets, respectively. The parameters derived from curve fitting were analyzed by PROC TTEST in SAS 9.4 (SAS Institute Inc., USA). The model included the parameter (amplitude, mean, or T_{max}) as a variable and the mouse type (i.e., *Six3*$^{fl/fl}$ and *Six3*^{syn}) as a class.

2.11. Sucrose preference test

As described previously [42], *Six3*^{syn} males and litter-mate controls were single housed in their home cage in LD, with two water bottles. One water bottle contained water, and a second water bottle contained 4% dissolved sucrose. Mice were habituated to the presence of two drinking bottles for 3 days in their home cage. Following acclimation, mice had the free choice of either drinking the 4% sucrose solution or plain water for a period of 4 days. The location of the bottles was switched each day to avoid a confounding factor of cage-side

preference. The water bottles were weighed daily and the change in weight was recorded.

2.12. Immunohistochemistry and hematoxylin & eosin (H&E) staining

Tissues were collected between ZT4 and ZT7 and fixed overnight at 4 °C in 60% ethanol, 30% formaldehyde, and 10% glacial acetic acid. Tissues were washed in 70% ethanol and embedded in paraffin. Single immunohistochemistry on 10 μm coronal brain sections embedded in paraffin was performed as previously described [43]. Primary antibodies were rabbit anti-vasoactive intestinal peptide (VIP, Immunostar #20077, 1:1000, RRID:AB_572270); rabbit anti-Somatostatin (SS) antibody (Immunostar #20067, dilution 1:500, RRID: AB_572264); and mouse anti-arginine vasopressin (AVP)-associated neurophysin (dilution 1:1000; PS41, Harold Gainer, NIH, Bethesda, MD, USA). Sections were incubated in 1:300 secondary anti-rabbit IgG (Vector Laboratories, #BA-1000). Immunohistochemistry for AVP followed a modified protocol incorporating additional steps for "mouse-on-mouse (M.O.M.)" blocking following vendor's recommendations (M.O.M. kit, Vector Laboratories). Secondary antibodies were purchased from Vector labs, and colorimetric VIP (purple staining) and DAB (brown staining) assays (Vector laboratories) revealed the primary antibodies. Total automated counts of neurons were done at 20× magnification by calculating the sum of SS, AVP or VIP expressing neurons on 2 sections (averaged) of brain tissue at Bregma −0.58, −0.72, −0.82 (SS staining in PVN); −0.32, −0.46, −0.58 (SS staining in PeVN); −0.46, −0.58, −0.72 (AVP staining in PVN) and −0.34, −0.46, −0.58 (SS, AVP and VIP staining in SCN).

2.13. Cell culture and transient transfections

NIH3T3 cells (American Type Culture Collection) were cultured in DMEM (Mediatech), containing 10% fetal bovine serum (Gemini Bio), and 1x penicillin-streptomycin (Life Technologies/Invitrogen) in a humidified 5% CO_2 incubator at 37 °C. For luciferase assays, NIH3T3 cells were seeded into 24-well plates (Nunc) at 30,000 cells per well. Transient transfections were performed using PolyJet™ (SignaGen Laboratories, Rockville, MD), following manufacturer's recommendations. NIH3T3 cells were co-transfected as indicated in the figure legend with 200 ng/well luciferase reporter plasmids, as well as 100 ng/well thymidine kinase-β-galactosidase reporter plasmid, which served as an internal control [44]. Six total Bmal1-luciferase plasmids were used. The full-length mouse Bmal1-luciferase reporter plasmid (Addgene, Plasmid #46824) was modified to remove an erroneous homeodomain binding site at −537 bp which does not appear in either the mouse genome or in the original depositor's sequence. This modified Bmal1-luciferase plasmid was used for all experiments. Site directed mutagenesis of the ATTA-like sites in the Bmal1-luciferase plasmid was performed using the NEB Q5 Site-Directed Mutagenesis Protocol (New England Biolabs Inc.), following manufacturer's instructions. Primers for mutagenesis were designed using NEBase Changer (Supplementary Table 2). The expression vector used was mouse Six3/pcDNA overexpression plasmid (200 ng/well, Origene Technologies, Rockville, MD). To equalize the amounts of DNA transfected into cells, we systematically equalized plasmid concentrations by adding the corresponding plasmid backbone. Cells were harvested 24 h after transfection in lysis buffer [100 mM potassium phosphate (pH 7.8) and 0.2% Triton X-100]. Luciferase values were normalized to β-galactosidase values to control for transfection efficiency. Values were further normalized by expression as fold change compared to pcDNA (the empty expression vector control plasmid), as indicated in the figure legend. Data represent mean ± SEM of at least five independent experiments done in triplicate.

2.14. Statistical analysis

Statistical analyses were performed with GraphPad Prism 8, using Student's t-test, one-way ANOVA or two-way ANOVA, followed by *post hoc* analysis by Tukey or Bonferroni as indicated in figure legends, with $p < 0.05$ to indicate significance. First peak phase relationships of Per2:LUC timing were analyzed in R via a Circular Analysis of Variance High Concentration F-Test, with a corrected confidence level of $p < 0.01667$ to account for family-wise error. Wheel-running activity was analyzed via a two-way repeated-measures ANOVA.

3. RESULTS

3.1. *Six3*^{syn} males have impaired SCN function, but intact fertility

We recently showed that the *Synapsin*^{cre}-allele recombines the *Six3*^{flox}-allele throughout the brain including the SCN, impairing SCN circadian output in *Six3*^{syn} females [25]. To determine whether circadian function was also weakened in *Six3*^{syn} males, we placed *Six3*$^{fl/fl}$ and *Six3*^{syn} males on running-wheels (Figure 1A). To limit the number of mice in the male wheel-running study, as it was an extension of our previous study in *Six3*^{syn} females, we decided to estimate the number of mice required to reach the lower power of 60% based on chi square amplitude (Qp) values of our previous publication studying wheel-running of *Six3*^{syn} females [25]. Our ad-hoc power analysis indicated that a total of 16 mice would allow us to achieve more than 60% of power. We first evaluated *Six3*^{syn} male activity on the running-wheels, as assessed through average wheel revolutions. *Six3*^{syn} males had comparable activity to *Six3*$^{fl/fl}$ during the lights ON and OFF of the habituation period (Hab. ON and Hab. OFF, Figure 1B), and during the baseline (LD) activity period following the habituation period (LD ON and LD OFF, Figure 1B). Running wheel activity is a known rewarding activity in rodents [45,46]. To determine whether the non-significant trend toward reduced activity of *Six3*^{syn} males during lights OFF (Figure 1B) reflected a global reduction in reward function, we performed a sucrose preference test in a new cohort of mice. *Six3*^{syn} mice presented with a sucrose preference over water comparable to *Six3*$^{fl/fl}$ mice, indicating overall normal reward processing of *Six3*^{syn} males (Figure 1C, 3-way ANOVA, effect genotype $F(1, 50) = 1.646$, $p = 0.206$). To determine whether the endogenous free-running period of the SCN was changed in *Six3*^{syn} mice, we evaluated the wheel-activity rhythm period. *Six3*^{syn} mice had a lengthened free-running period in DD as compared to *Six3*$^{fl/fl}$ (Tau, Figure 1D, 2-way ANOVA, effect of genotype $F(1,22) = 14.51$, $p < 0.001$). It should be noted that we observed a surprisingly large variation in Tau in the controls (Figure 1D), a variation that was even more pronounced in the *Six3*^{syn}. Indeed, as can be observed on the individual actigraphy data from 6 controls and 8 *Six3*^{syn} males (Supplementary Figure 1), the activity onset of the controls during DD was relatively variable, suggesting the *Six3*$^{fl/fl}$ allele by itself impacts SCN function. Interestingly, as we had previously observed for *Six3*^{syn} females [25], 6/8 *Six3*^{syn} males on DD had very variable activity periods, where they initially trended to have a period shorter than 24 h, but after variable times on DD, suddenly switched to a longer Tau. Owing to the low activity profile of some of the *Six3*^{syn} males (Supplementary Figure 1, *Six3*^{syn}), we were unable to analyze the data from some of the mice. The great variation in wheel-activity rhythm and activity levels of the *Six3*^{syn} males led to a great variation in the shortening/lengthening in Tau in DD of *Six3*^{syn} males, a

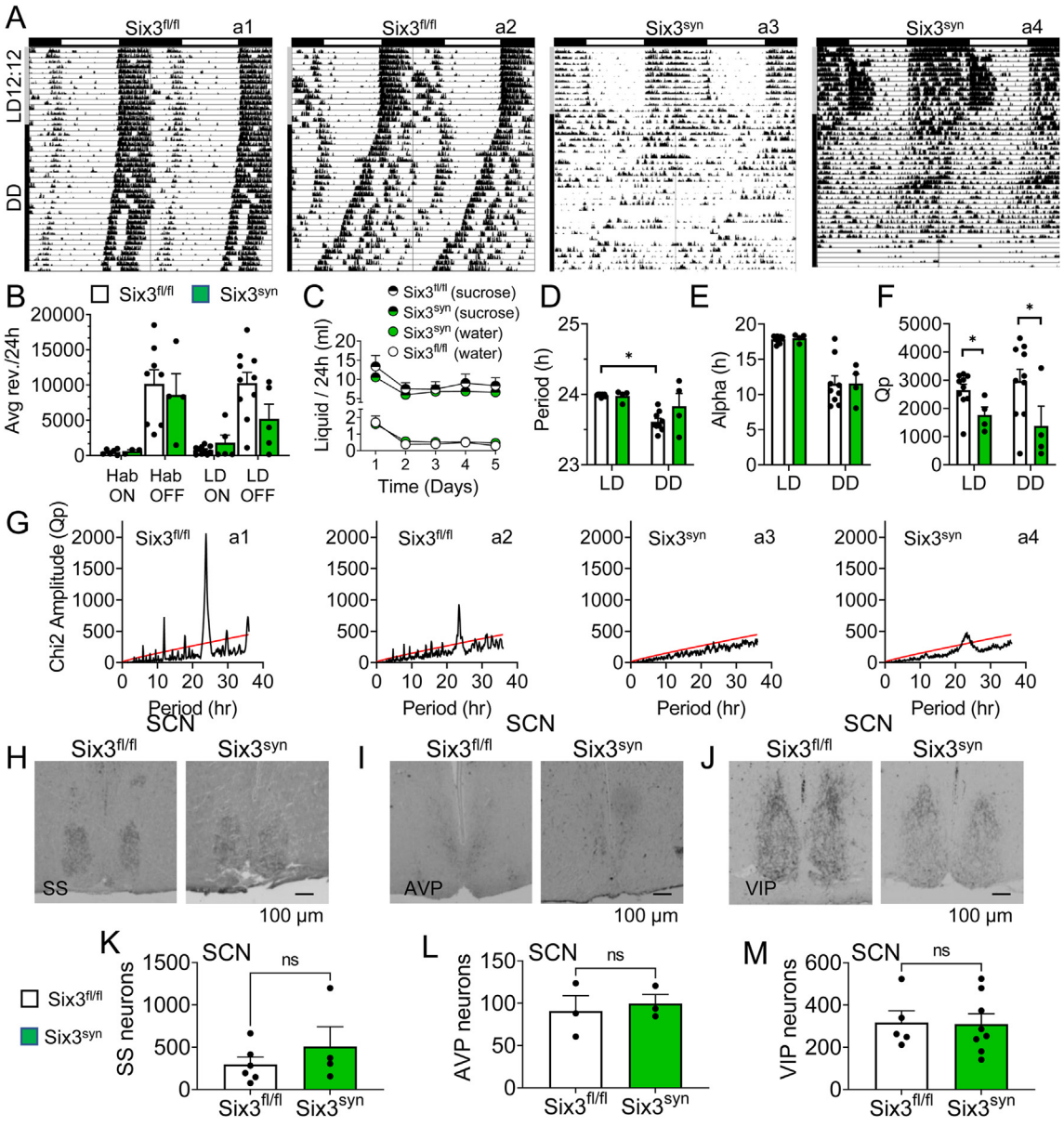

Figure 1: *Six3*^{syn} males have weakened wheel-running activity rhythms in DD. A) Double plotted actograms for representative *Six3*$^{fl/fl}$ and *Six3*^{syn} males. Data are presented in ClockLab normalized format. Horizontal bars above the actogram indicate lights ON (white) and lights OFF (black) during the LD cycle (12-h light, 12-h dark). *Six3*^{syn} males were in LD for 2 weeks (after an additional week of habituation in LD, not shown), followed by 4 weeks of DD, as shown by the gray/black vertical bars to the left of the actograms. Wheel-running patterns during LD and DD were analyzed for B) total wheel-running activity (average wheel revolutions per 24 h), during the habituation period (Hab), and LD during the 12 h with lights ON (ON) and 12 h of lights OFF (OFF), n = 5–10, D) circadian period, n = 4–10, E) alpha (activity duration), n = 4–10, and F) rhythm strength (Chi^2 periodogram Qp), n = 4–10. In B, histograms show 14-day average wheel-running data for LD and 7-day averaged data for habituation (Hab). G) Example chi^2 periodograms for the actograms shown in A (see matching codes (a1, a2, etc.) in the upper right corners of corresponding actograms and periodograms. C) Sucrose preference of *Six3*$^{fl/fl}$ and *Six3*^{syn} males, n = 6. (B, D, E, F) Two-way ANOVA mixed effect model. (C) 3-way ANOVA mixed effect model. Brackets indicate compared groups, *, $p < 0.05$. H-J) Illustrative immunohistochemistry images, and K-M) quantification of cell numbers of the indicated neuropeptides in the adult *Six3*$^{fl/fl}$ and *Six3*^{syn} male SCN. Student's t-test. $p > 0.05$, n = 3–8.

variation that also resulted in variable activity phase (alpha), which was comparable in *Six3*$^{fl/fl}$ and *Six3*^{syn} mice (Figure 1E, 2-way ANOVA, effect of genotype F (1,22) = 0.01, $p < 0.92$). To determine whether the lengthened Tau in *Six3*^{syn} was associated with weakened circadian timekeeping in the SCN, we evaluated circadian rhythm strength by chi square. *Six3*^{syn} had reduced chi square amplitude (Qp) in LD (Figure 1F) and DD (Figure 1F,G). SCN circadian output precision and strength are regulated by numerous factors, including SCN neuron connectivity. To determine whether the change in SCN output might be through an effect of SIX3 on the expression of SCN peptides, we evaluated SCN expression of somatostatin (SS), arginine vasopressin (AVP) and vasoactive intestinal polypeptide (VIP) by immunohistochemistry. No significant difference was observed in the number of SCN neurons expressing SS (Figure 1H,K), AVP (Figure 1I,L) or VIP (Figure 1J,M) in the *Six3*^{syn} males as compared to controls.

To determine whether the reduced SCN circadian precision was associated with changes in the molecular clock within SCN neurons, we analyzed the capacity of SIX3 to modulate the molecular clock genes *Per2* and *Bmal1* through *in vitro* transient transfection studies. We recently showed that SIX3 overexpression *in vitro* increased Per2-luciferase expression through ATTA-sites in the *Per2* regulatory region [25]. To determine whether SIX3 also regulates *Bmal1* expression, we analyzed the *Bmal1* regulatory region for potential SIX3 binding sites (ATTA-like sites) and identified five potential SIX3 binding sites (Supplementary Table 2). One potential binding site, located at −537 bp, was not present in either plasmid creator's original sequence or in any build of the mouse genome. As such, we modified the plasmid back to its correct sequence, leaving four potential homeodomain binding sites. To assay for SIX3 regulation of *Bmal1* expression, we transiently transfected NIH3T3 cells with the regulatory region of *Bmal1* driving luciferase (Bmal1-luciferase), with SIX3 or empty vector (pcDNA). SIX3 overexpression increased Bmal1-luciferase expression 2.3-fold (Figure 2A). To determine whether the enhanced expression of Bmal1-luciferase was mediated through the putative SIX3 binding sites, we created four plasmids with single ATTA-like sites mutated, in addition to one plasmid with all four ATTA-like sites mutated (ΔATTA). All the mutated ATTA sites impacted SIX3 regulation of Bmal1-luciferase expression (Figure 2A).

It is well established that changes in BMAL1 and PER2 impact circadian timekeeping. To determine if the capacity of SIX3 to regulate core clock gene expression *in vitro* translated into changes in circadian timekeeping function in SCN tissue, we generated triple transgenic mice, crossing *Six3*^{syn} mice with Per2:LUC knock-in reporter mice (*Six3*^{syn}*:Per2::LUC*). SCN slices from *Six3*^{syn}*:Per2::LUC* males had a longer circadian period than controls (Figure 2B,C), without significantly impacting Per2:LUC amplitude (Figure 2B,C). Changes in SCN period can impact circadian time-keeping in peripheral tissues. Per2:LUC period and amplitude were not significantly impacted in the pituitary or liver (Figure 2D,E), whereas a shortening in period, but no change in amplitude was observed in the epididymis (Figure 2F).

Weakened SCN output and changes in circadian timekeeping in reproductive tissues are associated with reduced female fertility [25,47,48], and loss of VIP impacts testis function [49]. To determine if the shortening of period in epididymal Per2:LUC rhythms (Figure 2F) was associated with impaired reproductive parameters, we first assessed pubertal onset through preputial separation. Preputial separation occurred at the same age in *Six3*$^{fl/fl}$ and *Six3*^{syn} mice (Figure 3A). Interestingly, around the age of pubertal onset (∼3-4 weeks-of-age), *Six3*^{syn} males had lower body weight than litter mate controls (Figure 3B). Despite the ∼2 fold reduction in body weight in males 12 weeks of age or older (Figure 3B), adult *Six3*^{syn} males generated litters of a comparable size to *Six3*$^{fl/fl}$ (Figure 3C), and in the hypothalmus at 6 and 12 weeks old males, the expression of *Gnrh1* (gonadotropin-releasing hormone, Figure 3D), a transcript required for GnRH production and fertility, was comparable to controls. GnRH acts on the pituitary to promote luteinizing hormone (LH) and follicle-stimulating hormone (FSH) production and release. In agreement with the normal *Gnrh1* transcript levels in the hypothlamus, pituitary *Lhb* and *Fshb* expression (Figure 3E,F), LH and FSH (Figure 3G,H), as well as testicular testosterone production [25], were comparable between *Six3*$^{fl/fl}$ and *Six3*^{syn} males at 6 and 12 weeks of age, except for a reduction of *Lhb* in *Six3*^{syn} at 6 weeks of age as compared to controls (Figure 3E).

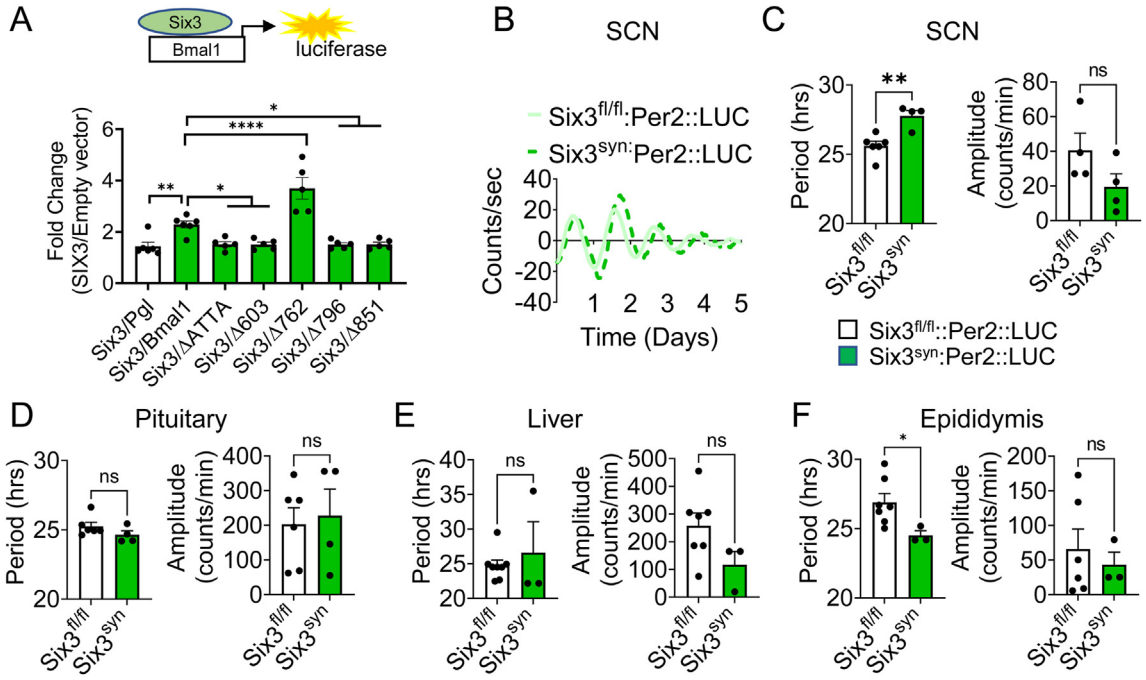

Figure 2: SIX3 regulates Bmal1-luciferase expression in NIH3T3 cells and Per2:LUC circadian period in explants of SCN and epididymis. A) Transient transfections of NIH3T3 cells with a reporter plasmid containing the mouse *Bmal1* regulatory region driving the expression of firefly luciferase (Bmal1-luciferase) with *Six3* overexpression vector (200 ng, green) or its empty vector (pcDNA 200 ng, white). Location of site-directed mutagenesis of ATTA and ATTA-like sites in the mouse Bmal1-luciferase plasmid are indicated with the Δ. For ΔATTA, all ATTA sites in the regulatory region have been mutated (see Supplementary Table 2). Statistical analysis by one-way ANOVA, with Dunnett's post-hoc analysis as compared to Six3/Bmal1-luciferase, *, $p < 0.05$; **, $p < 0.01$; ***, $p < 0.001$, $n = 5–6$ in triplicate. B) Example recording of SCN Per2:LUC circadian period. Histogram of Per2:LUC period and amplitude in the C) SCN, D) pituitary, E) liver and F) epididymis from *Six3*$^{fl/fl}$*:Per2::LUC* and *Six3*^{syn}*:Per2::LUC* males. Statistical analysis by Student's t-test, *, $p < 0.05$; **, $p < 0.01$, $n = 3–6$.

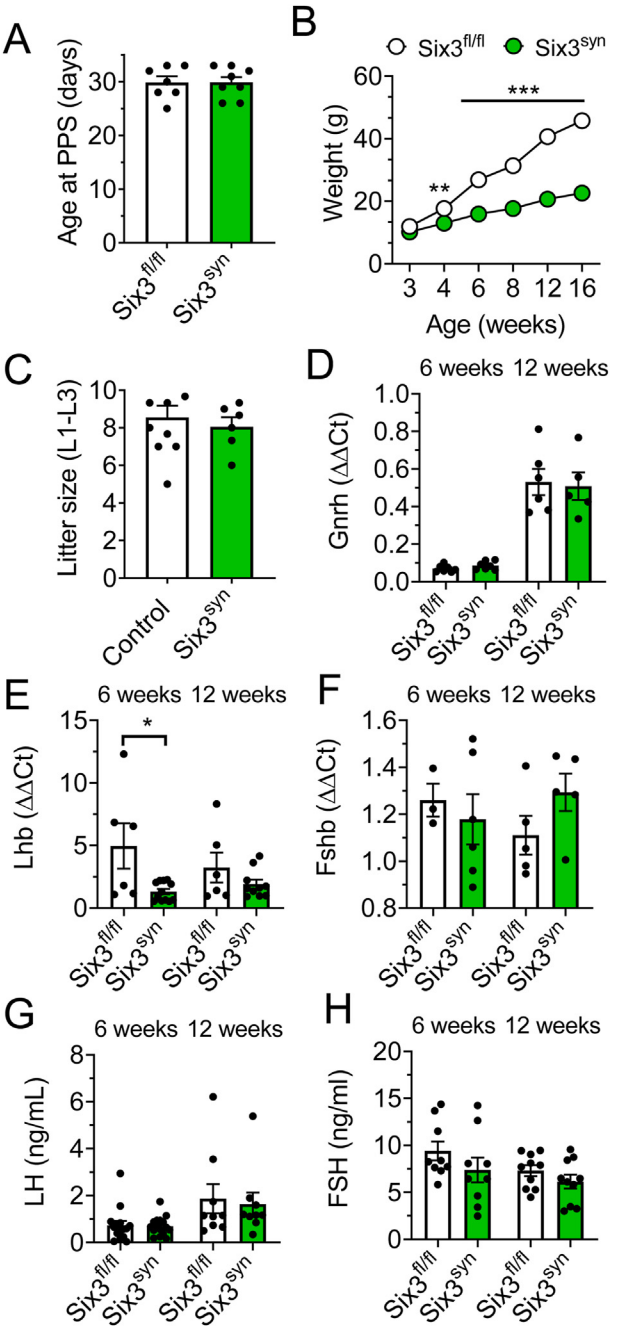

Figure 3: *Six3*^{syn} males gain less body weight during development yet maintain normal reproductive axis function and fertility. *Six3*$^{fl/fl}$ and *Six3*^{syn} males were evaluated for A) age at pubertal onset as determined by preputial separation (PPS), B) body weight during development, C) litter sizes (average of first three litters), D) *Gnrh1* mRNA levels in the hypothalamus, E) Lhb mRNA, F) Fshb mRNA in the pituitary, and circulating G) LH and H) FSH levels. Statistical analysis by (A, C–H) Student's t-test and (B) two-way ANOVA, repeated measures. $^{*}p < 0.05$, $^{**}p < 0.01$, $^{***}p < 0.001$. n = 4–16.

3.2. *Six3*^{syn} males have increased % lean mass, improved GTT, and increased metabolic rate

To further explore the ~50% reduction in body weight of adult *Six3*^{syn} males as compared to *Six3*$^{fl/fl}$ males (Figure 3B), we used dual energy X-ray absorptiometry (DEXA) to measure the body composition of 12-week-old male mice. As compared to *Six3*$^{fl/fl}$ males, *Six3*^{syn} males had significantly less total fat mass (Figure 4A), a lower % fat mass (Figure 4B), and less lean mass (Figure 4C), but increased lean mass as a percentage of total body mass (Figure 4D). To determine whether the increase in % lean mass was associated with improved glucose tolerance, we performed a glucose tolerance test (GTT) at 7, 12, and 18 weeks of age. No significant difference in fasted basal blood glucose levels were identified (Figure 4E). In contrast, at all the ages studied, *Six3*^{syn} males showed reduced blood glucose levels compared to *Six3*$^{fl/fl}$ (Two-way ANOVA, repeated measures). Effect of genotype: 7-weeks-of-age $F(1, 126) = 56.47$, $p < 0.0001$; 12-weeks-of-age $F(1, 42) = 58.20$, $p < 0.001$; 18-weeks-of-age $F(1, 42) = 86.62$, $p < 0.0001$.

We next examined whether hypophagia contributed to the reduced fat mass in these mice by using the comprehensive Lab Animal Monitoring System (CLAMS) metabolic cages. Consistent with a higher metabolic demand for a smaller animal [50], *Six3*^{syn} males had a higher metabolic rate than *Six3*$^{fl/fl}$ (Figure 5A–E), and ate more chow (Figure 5F,G), without eating for longer time periods (Figure 5H), but had normal energy expenditure (Figure 5I). In addition, *Six3*^{syn} males had increased locomotor activity, as evaluated using beam breaks in the metabolic cages (Figure 5J,K), and repetitive behavior during the dark phase compared to *Six3*$^{fl/fl}$ (Figure 5L). Consistent with the increased nocturnal activity (Figure 5J,K. K: Two-way ANOVA interaction genotype with time [$F(22, 220) = 2.278$], $p = 0.014$, n = 6), *Six3*^{syn} males had increased VO2 and VCO2 at night as compared to *Six3*$^{fl/fl}$ males (Figure 5B,D). Changes in locomotor activity and weakened SCN output can change the timing of peak VO2 and VCO2 rates [51]. To determine the time of day of peak VO2 and VCO2, we smoothed the VO2 and VCO2 data, and used a sinusoidal model to identify the rhythm phase (Figure 5M, N, example VO2 data illustrated, see Supplementary Figs. 2–5 for individually smoothed data sets and model fitting). We found no change in the phase (peak time) of VO2 (Figure 5O) or VCO2 (Figure 5P). To determine whether the dysregulated metabolic function might be driven, in part, by *Synapsin*^{cre} recombination of the *Six3*^{flox} allele in peripheral tissues, we tested for *Synapsin*^{cre}-driven *Six3*^{flox}-allele recombination. We confirmed that in males *Synapsin*^{cre} targets the hypothalamus and pituitary (Figure 5Q) and also identified recombination in the testis. No recombination was seen in white and brown adipose tissue, liver, tail or the pancreas (Figure 5Q). Of these tissues, *Six3* is known to be expressed in the hypothalamus, cortex, and pituitary (Figure 5Q, *) [18].

3.3. *Six3*^{syn} males have increased SS in the periventricular nucleus (PeVN)

Within the brain, metabolic control is regulated by the hypothalamus, where genes coding for neuropeptides known to be involved in metabolic homeostasis include *Npy* (neuropeptide Y), *Kiss1* (kisspeptin), *Ghrh* (growth hormone releasing hormone), and *Ss* (somatostatin) [4]. *Npy-, Kiss1-,* and *Ghrh*-expressing neurons are primarily located in the arcuate nucleus, whereas *SS* neurons are located in the PVN and PeVN (Figure 6. A-C). The arcuate nucleus, PVN, and PeVN are targeted by the *Synapsin*^{cre}-allele [25], and express *Six3* (Figure 6A–C). To determine what neuronal population(s) might be involved in the altered metabolic parameters of the *Six3*^{syn} males, we performed qPCR on the entire hypothalamus. At 6 weeks of age, but not at 12 weeks of age, *Six3*^{syn} males had a significant increase in hypothalamic expression of *Ss and Npy*, but no significant change in *Tshb, Ghrh* (Figure 6D–G), or receptors integrating metabolic status were observed (Figure 6H).

The limitation of using whole hypothalamus extracts for qPCR is the incapacity to detect moderate or small gene expression changes in discrete neuronal populations. To separate out the neuronal

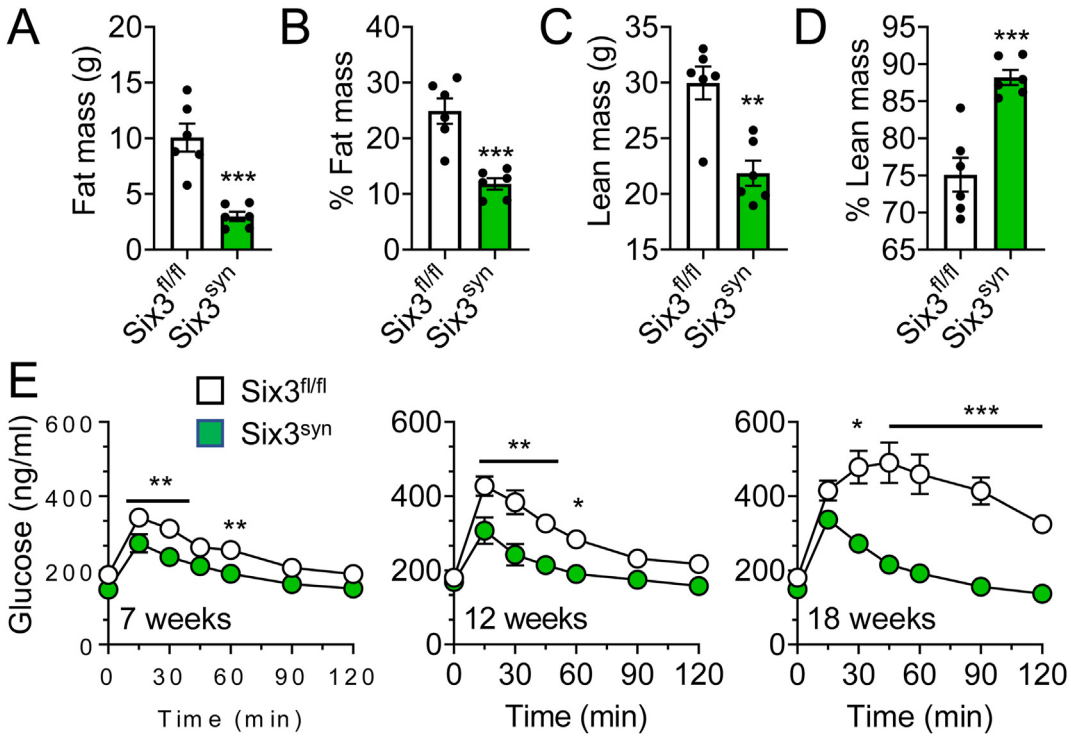

Figure 4: *Six3*^{syn} males have increased % lean body mass and improved glucose tolerance test. DEXA measurements of *Six3*^{syn} males fed standard chow had reduced A) total and B) % fat mass, C) reduced total lean mass, and D) increased % lean mass at 12 weeks of age. E) Glucose tolerance test (GTT) results (blood glucose after IP glucose challenge) in 7, 12, and 18-week-old males. Statistical analysis by (A–D) Student's t-test and (E) two-way ANOVA, repeated measures. $*p < 0.05$, $**p < 0.01$, $***p < 0.001$, n = 4–6.

population(s) contributing to the reduced growth and increased metabolic rate in *Six3*^{syn} males, we conditionally deleted *Six3* from kisspeptin neurons (*Six3*^{kiss}). We found that *Six3*^{kiss} males had comparable body weight to control (*Six3*$^{fl/fl}$) males from 3 to 12 weeks of age (Figure 6I), indicating the significant change in body weight developing after 4 weeks of age in *Six3*^{syn} males is unlikely to be driven by *Six3* in kisspeptin neurons. We therefore shifted our focus to AVP and SS expressing neurons of the PVN and PeVN which are known to regulate metabolic status and the growth axis [52,53]. Using immunohistochemistry, we found that *Six3*^{syn} males and *Six3*$^{fl/fl}$ controls had a comparable number of SS-expressing neurons in the PVN (Figure 6J, M), but *Six3*^{syn} males had a greater number of SS-expressing neurons in the PeVN compared to control mice (Figure 6K, N). The increased number of SS-expressing neurons in the PeVN provides a mechanism to regulate pituitary release of GH, a hormone critical in growth and metabolism. We also evaluated AVP expression in the PVN, as AVP neurons in the PVN have been associated with neuroendocrine regulation of metabolic function [53,54], and we previously found SIX3 to be a potent activator of *Avp* expression [25]. We did not, however, detect a change in AVP cell numbers in the PVN of *Six3*^{syn} males (Figure 6. L, O).

3.4. *Six3*^{syn} males have a dysregulated growth axis causing reduced body size and bone demineralization

SS is a known repressor of GH release (Figure 7A). To determine if the increase in SS in *Six3*^{syn} males impacted *Gh* mRNA, we performed qPCR of mRNA extracted from whole pituitary. At 6 weeks of age, but not 12 weeks of age, *Six3*^{syn} mice exhibited a significant decrease in expression of *Gh* (Figure 7B). In contrast, GH release was significantly increased at 12 weeks of age (Figure 7C). To further explore how the changes in body weight might be caused by abnormal GH release, we used qPCR to evaluate two liver transcripts regulated by GH: *Igf1* (insulin like growth factor 1) and *Ghr* (growth hormone receptor). We did not find a significant change in either *Igf1* (Figure 8A) or *Ghr* (Figure 8B) in the adult *Six3*^{syn} liver. Despite these non-significant changes of *Igf1* expression in the liver, it remains possible the IGF1 protein is reduced, as *Six3*^{syn} bone mineral count (Figure 8C) and bone mineral density (Figure 8D), were significantly reduced (see Figure 7A for summary of the growth axis).

4. DISCUSSION

Here, we demonstrate the novel role of SIX3 in the brain: conditional KO of *Six3* in post proliferative neurons (*Six3*^{syn}) is associated with reduced growth, increased lean mass, improved glucose tolerance, and weakened circadian wheel-running rhythms. These studies show for the first time the involvement of SIX3 in neuronal control of the growth axis and metabolic function and identify *Six3* as a gene that warrants further studies to focus on PeVN SS neurons and neuronal control of GH release.

4.1. Reduced growth and dwarfism in Six3^{syn} males

The most striking phenotype of the *Six3*^{syn} males was their significant reduction in growth starting at 4 weeks of age, which was associated with increased % lean mass and reduced fat mass. As we recently described, conditional KO of *Six3* in kisspeptin neurons (*Six3*^{kiss}) resulted in reduced fertility [30]; therefore, we first tested whether this metabolic deregulation was caused by loss of SIX3 in the arcuate nucleus. We did not find any significant changes in arcuate nucleus mRNA expression for peptides or receptors regulating or sensing

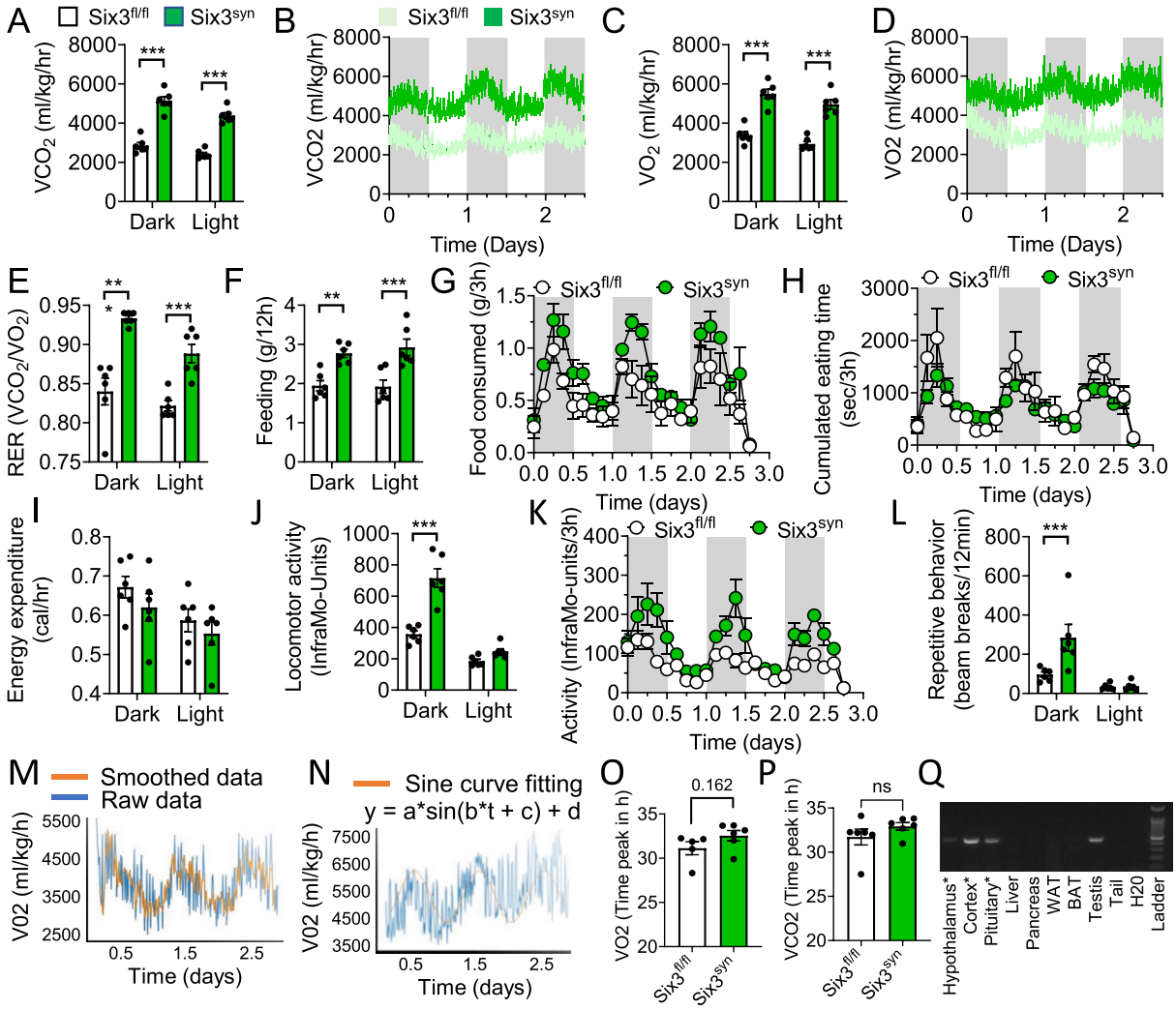

Figure 5: *Six3*^{syn} males have increased metabolic rates. CLAMS cage assessment of feeding, metabolism, and locomotor activity in 12-week-old *Six3*^{syn} males fed standard chow. A, B) CO_2 production (VCO2), C, D) O_2 consumption (VO2), E) respiratory exchange ratio (RER), F–H) feeding, I) energy expenditure, J, K) locomotor activity, and L) stereotypic repeated behavior. M, N) Example of smoothing and sine curve fitting to the VO2 data. O) VO2 and P) VCO2 phase (time of day of first peak) as estimated using the sine curve fitting to the smoothed data. Q) PCR to assay *Synapsin*^{cre} driven recombination of the *Six3*^{flox} allele in males. * indicated tissues known to express *Six3*. Abbreviations: WAT: white adipose tissue, BAT: brown adipose tissue. Statistical analysis by two-way ANOVA, repeated measures (A, C, E-K), and (O, P) Student's t-test. $^{**}p < 0.01$, $^{***}p < 0.001$. n = 5–6.

metabolic status, such as leptin receptor, insulin receptor, or the orexigenic *Pomc*, whereas a small but significant increase in the orexigenic *Npy* (neuropeptide Y) was detected at 6, but not 12 weeks of age [52,55–58]. Sucrose preference test performance was unaltered in *Six3*^{syn} males. Indeed, the hyperphagia of *Six3*^{syn} males correlated with increased metabolic rate, as expected for smaller, hyperactive animals [50]. These findings indicate that the reduced growth was not caused by dysregulated arcuate nucleus function. Rather, our data point to a novel role of SIX3 in PeVN SS neurons. A balanced release of arcuate GHRH, which defines the GH amplitude [59] and PeVN SS, which drives troughs of GH release [60,61], are well known to be required for normal growth, and suppression of GH in prepubertal mice is a leading cause of dwarfism [62]. Ideally, we would have studied the pulsatile release of GH in the *Six3*^{syn} males; however, as GH pulsatile release in males is characteristic of one GH pulse per ~2–4 h [37], we decided not to collect serial blood samples from *Six3*^{syn} males, as their significantly smaller size, and resulting smaller blood volume as compared to controls, made this approach unfeasible in this mouse line. Alternatively, we compared GH levels at a single time point to SS and GHRH expression in the brain as an indicator of how GH release was impacted in *Six3*^{syn} males. In agreement with the known repressive role of SS on GH release (Figure 7A), we found that *Six3*^{syn} males had increased expression of *Ss* mRNA in the hypothalamus at 6-weeks of age, an increase that trended in 12-week-old males on the transcriptional level (*Ss*, p = 0.076) and was significantly increased when counting SS expressing neurons in the PeVN. The significant increase in *Ss* in the 6-week-old *Six3*^{syn} males was associated with a significant reduction in *Gh* transcript, whereas circulating levels of GH was comparable to controls. The comparable levels of GH between *Six3*$^{fl/fl}$ and *Six3*^{syn} might be caused by the timing of blood collection, potentially happening during GH troughs. This possibility is supported by the reduction in *Gh* transcript, which is not pulsatile, and which correlated with stunted growth in young adult males, and dwarfism in adulthood. Interestingly in 12-week-old *Six3*^{syn} males GH levels were

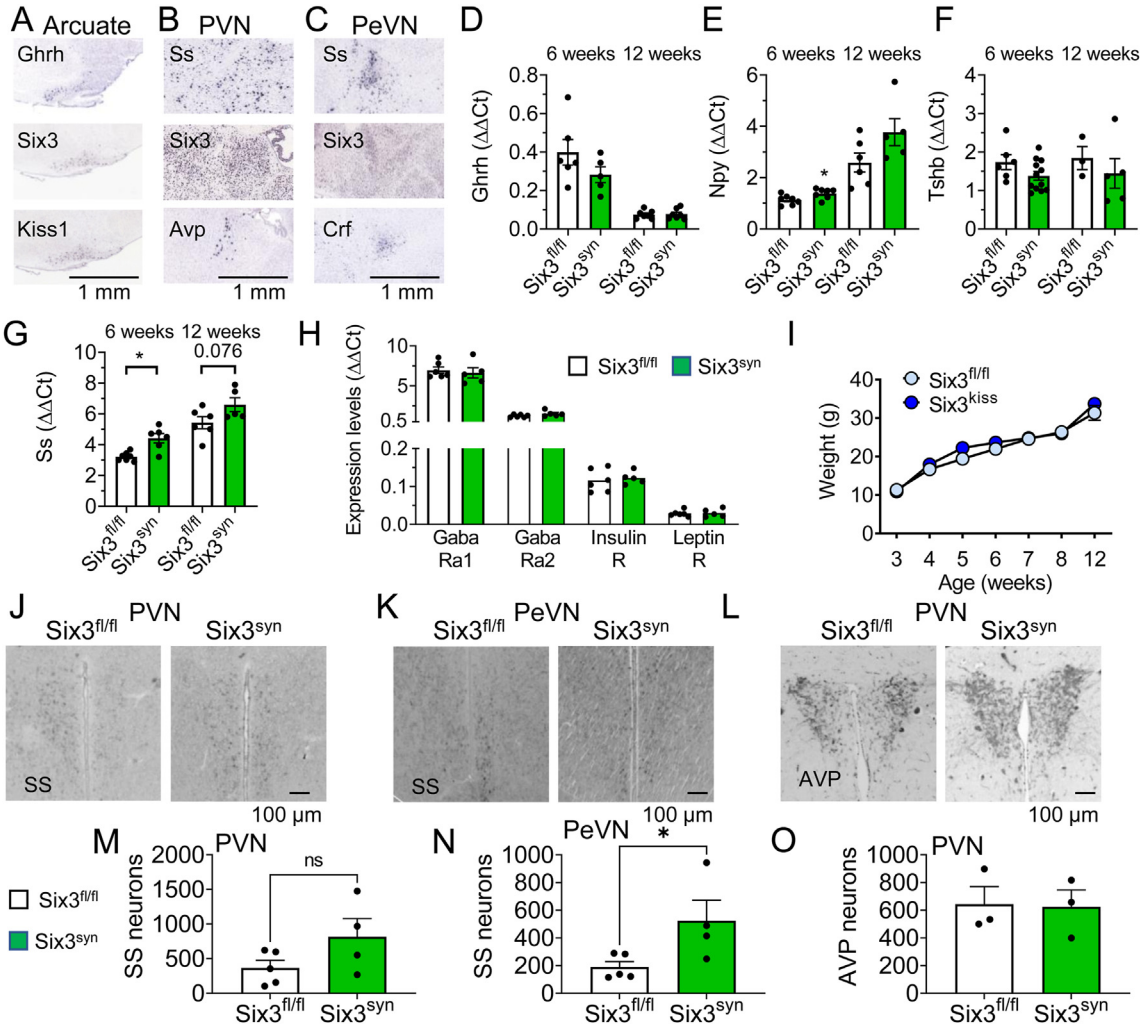

Figure 6: *Six3*^{syn} males exhibit increased SS levels in the hypothalamus. A-C) Allen Brain Atlas ISH images showing the expression of labeled genes in the adult male arcuate nucleus, PVN, and PeVN. For image information, see Supplementary Table 3. D-H) qPCR measurements of mRNA levels for *Ghrh*, *Npy*, *Tshb*, *Ss*, *GabaRa1, GabaRa2, Insulin R, and Leptin R* in whole hypothalamus of 6- and −12-week-old *Six3*$^{fl/fl}$ and *Six3*^{syn} males. Student's t-test, $*p < 0.05$, n = 5−6. I) Body weight of 3−12-week-old *Six3*$^{flox/flox}$ (*Six3*$^{fl/fl}$) and *Six3*$^{flox/flox}$:*Kiss*^{cre} (*Six3*^{kiss}) males. Two-way ANOVA, repeated measures, $p > 0.05$, n = 2−18. J-L) Illustrative immunohistochemistry images, and M−O) quantification of cell numbers of the indicated neuropeptides in the adult *Six3*$^{fl/fl}$ and *Six3*^{syn} male PVN and PeVN. Student's t-test. $*p < 0.05$, n = 3−5. Abbreviations: *Kiss1*: kisspeptin, *Avp*: arginine vasopressin, *Crf*: corticotropin releasing factor, *Ghrh*: growth hormone-releasing hormone, *Npy*: neuropeptide Y, *Tshb*: thyroid stimulating hormone β, *Ss*: somatostatin, *GabaRa1*: Gamma-aminobutyric acid receptor subunit alpha-1, *GabaRa2*: Gamma-aminobutyric acid receptor subunit alpha-2, *Insulin R*: insulin receptor, *Leptin R*: Leptin receptor.

higher than controls. This seemingly contradictory finding can be explained by two independent mechanisms. First, it is again possible the single blood collection time point led us to collect blood in *Six3*$^{fl/fl}$ only during GH troughs, whereas half of the blood samples collected from the *Six3*^{syn} were randomly collected during GH peaks. A second more plausible explanation is that the trending reduction in liver *Igf1* promoted GH secretion from the pituitary [63,64], counteracting the increased inhibitory tone by SS on somatotrophs. Although we did not measure circulating IGF1 in this study, *Six3*^{syn} liver *Igf1* mRNA levels trended downward, and two functional parameters enhanced by IGF1 were significantly reduced (bone mineralization and muscle mass, Figure 7A). Thus, we can infer from our data that adult *Six3*^{syn} males likely had impaired IGF1 feedback to the brain and pituitary, leading to increased GH release in adulthood, despite increased SS in the PeVN. Taken together, these findings support the known differential role of GH in early life versus adult and aging rodents [65]. Increased GH release in adulthood can be driven by reduced IGF1 negative feedback to the hypothalamus and somatotrophs. The dysregulated GH release in *Six3*^{syn} would also be expected to change expression of additional liver genes. What such genes are and how they contribute to the dysregulated metabolic function would be of great interest to explore in the future. Indeed, ~90% of sexually dimorphic genes in the liver are regulated by pulsatile GH patterns [66]. Thus, additional studies exploring how GH release patterns differ in *Six3*^{syn} males and females and how they contribute to changes in liver function would be of interest but are outside the scope of the present work.

Another important role of GH is its direct regulation of adipocyte function through the GH receptor. GH binding to its receptor promotes breakdown of triglycerides, thus increasing energy availability, while concomitantly suppressing the uptake of circulating lipids into adipocytes. Consistent with the increased GH release in 12-week-old *Six3*^{syn} males was their significant reduction of fat mass and increased % lean mass. The increase in % lean mass, along with the known role of GH in regulating glucose metabolism, resulted in improved glucose tolerance

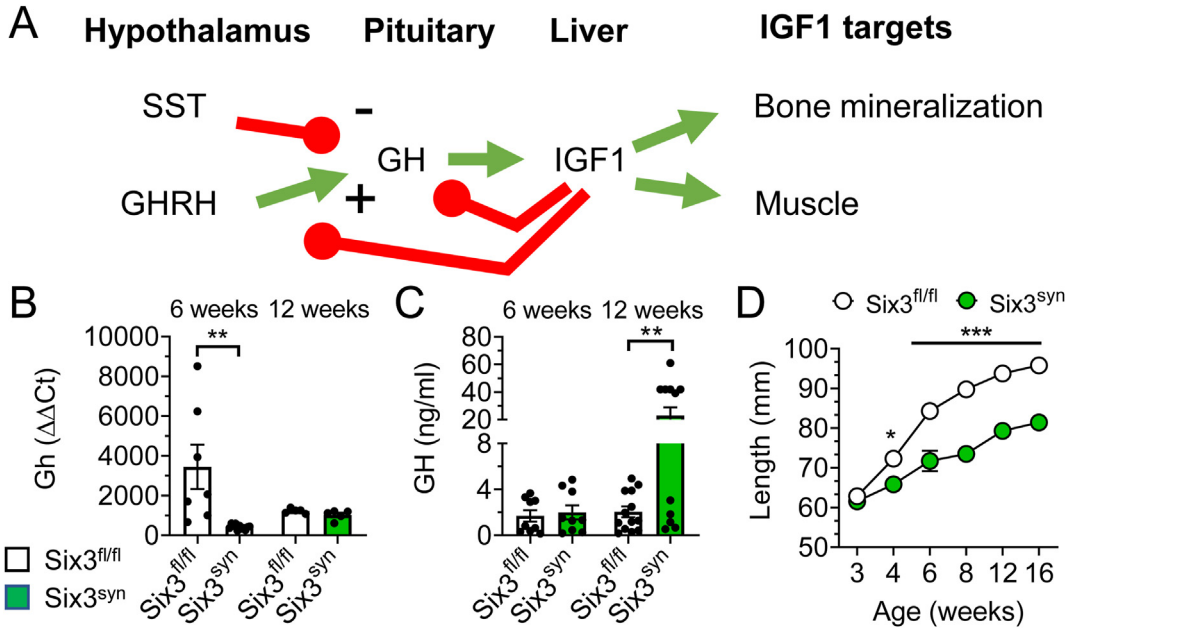

Figure 7: *Six3^{syn}* males exhibit reduced GH release and reduced body length. A) Simplified schematic of the neuroendocrine axis regulating growth. B) Pituitary qPCR for *Gh* and C) circulating GH in adult *Six3$^{fl/fl}$* and *Six3^{syn}* 6- and 12-week-old males. D) Body length of *Six3$^{fl/fl}$* and *Six3^{syn}* males at 3- to 16 weeks of age. (B, C) Student's t-test, and (D) Two-way ANOVA, repeated measures, $^{*}p < 0.05$, $^{**}p < 0.01$, $^{***}P < 0.001$, n = 4–9. Abbreviations: SS: somatostatin, GHRH: growth hormone releasing hormone, GH: growth hormone, IGF1: Insulin-like growth factor 1.

in *Six3^{syn}* males as compared to controls, an improvement that increased with age. Taken together, these data point to a novel role of SIX3 in regulating the growth axis through regulation of SS neurons. It will be of interest in future studies to specifically delete *Six3* in PeVN neurons in prepubertal and adult males to better understand the differential role of SIX3 in juvenile and adult animals in the regulation of the growth axis, fat versus lean body mass, and metabolic function.

4.2. Weakened SCN output contrasts with increased locomotor activity and metabolic rate in Six3^{syn} males

SIX3 is required for SCN development [24] and for SCN circadian timekeeping in females [25]. Consistent with these previous results in female mice, we found that *Six3^{syn}* males had weakened SCN output as measured by wheel-running activity rhythms. Interestingly, although the initial circadian period in DD was not significantly lengthened in *Six3^{syn}* as compared to *Six3$^{fl/fl}$* mice, 6 out of 8 *Six3^{syn}* males showed a lengthening of period from <24h to >24h during DD, and this period lengthening was reflected in PER2:LUC recordings of SCN explants. These data are consistent with our previous finding of a general lengthening of SCN circadian period in *Six3^{syn}* females, attributable to a direct action of SIX3 on the *Per2* promoter [25]. We show here that SIX3 also promotes Bmal1-luciferase expression *in vitro* and identify 4 ATTA sites required for this transcriptional activity. An additional contributing factor to the lengthening in SCN period in the *Six3^{syn}* is a possible change in neuropeptide expression. *In vitro*, SIX3 is an activator of the Avp-luciferase, but not the Vip-luciferase promoter, whereas it is unknown if SIX3 can directly regulate *Ss* expression. Using immunohistochemistry, we did not observed differences for AVP, VIP, or SS in *Six3^{syn}* SCN as compared to control. However, it remains possible that altered AVP, VIP, or SS release patterns could contribute to changes in SCN network function and output in these mice.

Impaired circadian time keeping is known to be a risk factor for obesity and metabolic dysfunction. SCN ablation causes increased insulin resistance, glucose intolerance, and weight gain [67]. But the relationship between circadian regulation and metabolism is probably complex. For instance, a high fat diet can blunt the normal circadian release of dopamine in the region around the SCN, and this may at least partly mediate its detrimental metabolic effects [67]. In our study, it is unclear how the weakened SCN output in *Six3^{syn}* males might be related to the improved glucose tolerance and reduced fat mass, which is not what would be predicted based on the simple hypothesis that weakened SCN circadian output impairs metabolic function.

Circadian effects on metabolism may depend on phase rather than simply strength of SCN circadian output. Indeed, VO2 and VCO2 phase mis-alignment in transgenic mice has previously been observed in mice lacking SCN VIP-VPAC2 signaling [51], where these mice presented a phase advance in their daily rhythms of metabolism and feeding [51]. Interestingly, this phase advance in feeding was associated with reduced metabolic rates. Although our data trended toward phase delays (VO2, p = 0.162, Figure 5O), we did not find significant phase differences in the peak times of VO2 or VCO2 in *Six3^{syn}* mice vs. controls.

Another possible explanation for the improved metabolic status despite apparently weakened SCN circadian output is the increased nocturnal activity of *Six3^{syn}* males (observed in the metabolic cages, but not on the running wheels), which might actually indicate a selective strengthening of SCN rhythmic output. It is important to note two major differences between metabolic and wheel-running cages, which differed by size, and the absence/presence of a running wheel, respectively. The increase in nocturnal activity in the metabolic cages, was associated with increased repetitive behavior, which might indicate nocturnal neuronal hyperexcitability causing increased repetitive behavior. Together, this increase in nocturnal activity could provide a strengthened metabolic signal to the body, overriding the weakened SCN circadian strength. Indeed, exercise is known to alter clock gene expression in muscle and several other peripheral tissues, and timed

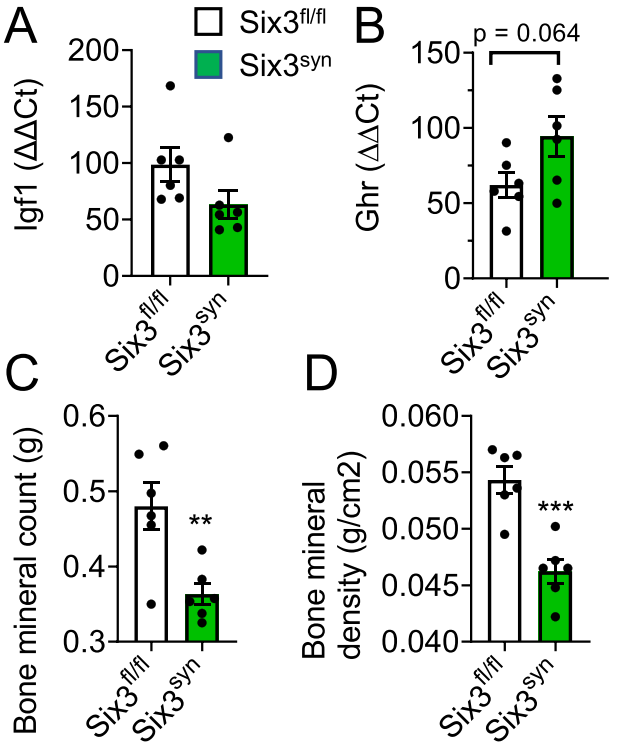

Figure 8: *Six3*^{syn} males exhibit reduced bone density and mineralization. A, B) qPCR for liver *Igf1* and *Ghr* in 12–16-week-old *Six3*$^{fl/fl}$ and *Six3*^{syn} males. DEXA measurements of *Six3*$^{fl/fl}$ and *Six3*^{syn} males fed standard chow revealed reduced C) bone mineral count, and D) bone mineral density. Student's t-test, $^{**}p < 0.01$, $^{***}p < 0.001$, n = 6. Abbreviations: *Ghr*: growth hormone receptor, *Igf1*: Insulin-like growth factor 1.

exercise combined with light therapy or food entrainment can be a potent circadian synchronizer [68–70]. Or perhaps the improved metabolism despite apparently weakened SCN circadian output involves the deletion of *Six3* in the striatum of *Six3*^{syn} mice. SIX3 is known to be involved in striatal medium spiny neuron plasticity and striatum function [27–29]. As the striatum is important for motor function and reward behavior, it would be of interest to specifically evaluate wheel-running patterns and metabolism in mice with *Six3* deletion only in striatal medium spiny neurons.

4.3. Six3^{syn} males have normal fertility

Despite their stunted growth and deregulation of the growth axis, *Six3*^{syn} males had normally timed pubertal onset and a normally functioning reproductive axis, with normal hypothalamic expression of *Gnrh1* supporting normal gonadotropin hormone production and release. This agrees with our previous report showing that *Six3*^{syn} males generate a comparable number of litters to *Six3*$^{fl/fl}$ in a fertility assay [25]. The maintenance of fertility in *Six3*^{syn} males is in striking contrast to the sub-fertility or infertility of female *Six3*^{syn} mice, which is due to loss of SCN gating of the LH surge to the proper time of day, and consequent failure to ovulate [25]. Interestingly, we found a shorter free-running circadian period in the epididymis of *Six3*^{syn} males, but this did not impact overall male fertility, so the possible function of local circadian clocks in this tissue is unclear. Circadian expression of core clock genes has also been found previously in other male reproductive tissues. In extra-testicular ducts and accessory tissues [71], the clock gene *Bmal1* may regulate the production of testosterone [72], but this hormone is present at normal levels in *Six3*^{syn} mice [25].

4.4. Value and limits of the Six3^{syn} mouse model to study neuronal maturation and function

Using conditional KO mice (Cre-LoxP system) comes with numerous potential caveats to consider in data interpretation [43,73–78]. We have recently further validated the effectiveness of the *Synapsin*^{cre}-allele for inducing recombination of the *Six3*^{flox}-allele throughout the brain, including the SCN, PVN, and PeVN [25]. Importantly, we did not observe any effects on brain peptide expression or behavioral measures in mice heterozygous for *Synapsin*^{cre}, providing reassurance that this allele on its own does not significantly alter neuronal function [25]. We here extend our previous study and show the *Synapsin*^{cre}-allele recombines *Six3*^{flox} in the male hypothalmus, cortex, pituitary and testis. Of these tissues, *Six3*^{flox} is known to be expressed in brain (hypothalamus and cortex), and pituitary. The identifed recombination in the testis contrasts with our previous report, where we did not find *Synapsin*^{cre}-allele recombination in the testis. This discrepancy could be due to the flox-allele recombined where the Rosa-allele used as a reporter for *Synapsin*^{cre}-driven recombination might be less efficiently recombined by *Synapsin*^{cre} than the *Six3*^{flox}-allele, not allowing us to detect recombination in the testis in our previous study [25]. We do not know if *Synapsin*^{cre} targets somatotrophs, a cell population that expresses *Six3* (personal correspondence with authors from Ho et al., 2020) [79]. Although we cannot rule out the possibility that *Six3* might have been deleted from a small number of somatotrophs, *Six3*^{syn} males produced and secreted GH in a pattern consistent with the observed changes in SS. This indicates that somatotroph function was not substantially impaired in our *Six3*^{syn} males.

Despite some limitations, the broad targeting of the *Synapsin*^{cre} allele in post-proliferative neurons provides a powerful tool to manipulate both maturing and mature neurons throughout the period of neuronal proliferation, which can dilute the effects of more conventional approaches. The specificity of targeting to later developmental stages is a particular advantage when studying genes, such as SIX3, that are highly expressed from early development through adulthood, and whose developmental loss can induce major brain defects obscuring any later effects. Thus, in this initial study, our aim was to obtain an overall picture of physiological functions of SIX3 in post proliferative neurons, rather than to elucidate the precise roles of *Six3* within specific neuronal populations. For this broad objective, the broad targeting of *Synapsin*^{cre} in the brain provided an excellent tool to identify the novel roles of Six3 in neurons.

4.5. Conclusion and future directions

Owing to broad expression of *Synapsin*^{cre} in the brain, allowing deletion of *Six3* after neuronal proliferation, we have identified the novel roles of SIX3 in maturing and mature neurons, where we show it is required from ~4 weeks of age onward to regulate growth. Specifically, our data point to the novel role of SIX3 in the PeVN, where it appears to be a regulator of SS neuron numbers and metabolism. This study lays the foundation for future studies focusing more specifically on the mechanisms by which SIX3 acts within hypothalamic regions including PVN, PeVN, and SCN to regulate metabolic status and circadian rhythms.

ACKNOWLEDGMENTS

This work was supported by National Institutes of Health (NIH) Grants R01 HD072754, R01 HD100580, and R01 HD082567 (to P.L.M.). It was also supported by NIH/Eunice Kennedy Shriver National Institute of Child Health and Human Development (NICHD) P50 HD012303 as part of the National Centers for Translational Research in Reproduction and Infertility (P.L.M.). P.L.M. was also partially supported

by P30 DK063491, P30 CA023100, and P42 ES010337. H.M.H. was partially supported by K99/R00 HD084759 and the United States Department of Agriculture National Institute of Food and Agriculture Hatch project MICL1018024. S.N.L. was partially supported by P42 ES010337, T32 GM008666, and a supplement to P50 HD012303. J.C. was partially supported by T32 HD007203 and K12 GM068524. J.A.B. was partially supported by the Frontiers of Innovation Scholars Program, UC San Diego. Work in the D.K.W. laboratory was supported by a Veterans Affairs Merit Award (I01 BX001146). Work in the M.R.G. laboratory was supported by Office of Naval Research N00014-13-1-0285. We thank Erica L. Schoeller, Alexandra M. Yaw, and Ichiko Saotome for assistance and feedback on the manuscript. We thank Peng Hu for his correspondence regarding their single cell RNA-seq analysis of 8-week-old mouse pituitaries and Dr. Harold Gainer (NIH, Bethesda, MD, USA) for the mouse AVP-associated neurophysin antibody.

CONFLICT OF INTEREST

None declared.

APPENDIX A. SUPPLEMENTARY DATA

Supplementary data to this article can be found online at https://doi.org/10.1016/j.molmet.2021.101431.

REFERENCES

[1] World Health Organization, 2021. Obesity and overweight (WHO fact sheet).
[2] Calle, E.E., Rodriguez, C., Walker-Thurmond, K., Thun, M.J., 2003. Overweight, obesity, and mortality from cancer in a prospectively studied cohort of U.S. adults. New England Journal of Medicine 348(17):1625–1638.
[3] Kim, S.H., Després, J.P., Koh, K.K., 2016. Obesity and cardiovascular disease: friend or foe? European Heart Journal 37(48):3560–3568.
[4] Timper, K., Brüning, J.C., 2017. Hypothalamic circuits regulating appetite and energy homeostasis: pathways to obesity. Dis Model Mech 10(6):679–689.
[5] Shi, S.Q., Ansari, T.S., McGuinness, O.P., Wasserman, D.H., Johnson, C.H., 2013. Circadian disruption leads to insulin resistance and obesity. Current Biology 23(5):372–381.
[6] Turek, F.W., Joshu, C., Kohsaka, A., Lin, E., Ivanova, G., McDearmon, E., et al., 2005. Obesity and metabolic syndrome in circadian Clock mutant mice. Science 308(5724):1043–1045.
[7] Roenneberg, T., Allebrandt, K.V., Merrow, M., Vetter, C., 2012. Social jetlag and obesity. Current Biology 22(10):939–943.
[8] Parsons, M.J., Moffitt, T.E., Gregory, A.M., Goldman-Mellor, S., Nolan, P.M., Poulton, R., et al., 2015. Social jetlag, obesity and metabolic disorder: investigation in a cohort study. International Journal of Obesity 39(5):842–848.
[9] Garaulet, M., Gómez-Abellán, P., Alburquerque-Béjar, J.J., Lee, Y.C., Ordovás, J.M., Scheer, F.A., 2013. Timing of food intake predicts weight loss effectiveness. International Journal of Obesity 37(4):604–611.
[10] Dauchy, R.T., Blask, D.E., Hoffman, A.E., Xiang, S., Hanifin, J.P., Warfield, B., et al., 2019. Influence of daytime LED light exposure on circadian regulatory dynamics of metabolism and physiology in mice. Comparative Medicine 69(5):350–373.
[11] Fleury, G., Masís-Vargas, A., Kalsbeek, A., 2020. Metabolic implications of exposure to light at night: lessons from animal and human studies. Obesity 28(S1):S18–S28.
[12] Charlot, A., Hutt, F., Sabatier, E., Zoll, J., 2021. Beneficial effects of early time-restricted feeding on metabolic diseases: importance of aligning food habits with the circadian clock. Nutrients 13(5):1405.
[13] Bonnefond, A., Raimondo, A., Stutzmann, F., Ghoussaini, M., Ramachandrappa, S., Bersten, D.C., et al., 2013. Loss-of-function mutations in SIM1 contribute to obesity and Prader-Willi-like features. Journal of Clinical Investigation 123(7):3037–3041.
[14] Ramachandrappa, S., Raimondo, A., Cali, A.M., Keogh, J.M., Henning, E., Saeed, S., et al., 2013. Rare variants in single-minded 1 (SIM1) are associated with severe obesity. Journal of Clinical Investigation 123(7):3042–3050.
[15] Bando, H., Brinkmeier, M.L., Castinetti, F., Gergics, P., Mortensen, A.H., Ozel, A.B., et al., 2020. SAT-291 SIX3 is essential for hypothalamic and pituitary development. Journal of the Endocrine Society 4(Supplement_1).
[16] Oliver, G., Mailhos, A., Wehr, R., Copeland, N.G., Jenkins, N.A., Gruss, P., 1995. Six3, a murine homologue of the sine oculis gene, demarcates the most anterior border of the developing neural plate and is expressed during eye development. Development 121(12):4045–4055.
[17] Anderson, A.M., Weasner, B.M., Weasner, B.P., Kumar, J.P., 2012. Dual transcriptional activities of SIX proteins define their roles in normal and ectopic eye development. Development 139(5):991–1000.
[18] Conte, I., Morcillo, J., Bovolenta, P., 2005. Comparative analysis of Six 3 and Six 6 distribution in the developing and adult mouse brain. Developmental Dynamics 234(3):718–725.
[19] Geng, X., Acosta, S., Lagutin, O., Gil, H., Oliver, G., 2016. Six3 dosage mediates the pathogenesis of holoprosencephaly. Development 143(23):4462–4473.
[20] Lagutin, O.V., Zhu, C.C., Kobayashi, D., Topczewski, J., Shimamura, K., Puelles, L., et al., 2003. Six3 repression of Wnt signaling in the anterior neuroectoderm is essential for vertebrate forebrain development. Genes & Development 17(3):368–379.
[21] Dubourg, C., Lazaro, L., Pasquier, L., Bendavid, C., Blayau, M., Le Duff, F., et al., 2004. Molecular screening of SHH, ZIC2, SIX3, and TGIF genes in patients with features of holoprosencephaly spectrum: mutation review and genotype-phenotype correlations. Human Mutation 24(1):43–51.
[22] Pasquier, L., Dubourg, C., Blayau, M., Lazaro, L., Le Marec, B., David, V., et al., 2000. A new mutation in the six-domain of SIX3 gene causes holoprosencephaly. European Journal of Human Genetics 8(10):797–800.
[23] Pasquier, L., Dubourg, C., Gonzales, M., Lazaro, L., David, V., Odent, S., et al., 2005. First occurrence of aprosencephaly/atelencephaly and holoprosencephaly in a family with a SIX3 gene mutation and phenotype/genotype correlation in our series of SIX3 mutations. Journal of Medical Genetics 42(1):e4.
[24] VanDunk, C., Hunter, L.A., Gray, P.A., 2011. Development, maturation, and necessity of transcription factors in the mouse suprachiasmatic nucleus. Journal of Neuroscience 31(17):6457–6467.
[25] Hoffmann, H.M., Meadows, J.D., Breuer, J.A., Yaw, A.M., Nguyen, D., Tonsfeldt, K.J., et al., 2021. The transcription factors SIX3 and VAX1 are required for suprachiasmatic nucleus circadian output and fertility in female mice. Journal of Neuroscience Research 99(10):2625–2645.
[26] Lavado, A., Oliver, G., 2011. Six3 is required for ependymal cell maturation. Development 138(24):5291–5300.
[27] Xu, Z., Liang, Q., Song, X., Zhang, Z., Lindtner, S., Li, Z., et al., 2018. SP8 and SP9 coordinately promote D2-type medium spiny neuron production by activating Six3 expression. Development 145(14):dev165456.
[28] Yang, L., Su, Z., Wang, Z., Li, Z., Shang, Z., Du, H., et al., 2021. Transcriptional profiling reveals the transcription factor networks regulating the survival of striatal neurons. Cell Death & Disease 12(3):262.
[29] Song, X., Chen, H., Shang, Z., Du, H., Li, Z., Wen, Y., et al., 2021. Homeobox gene Six3 is required for the differentiation of D2-type medium spiny neurons. Neurosci Bull 37(7):985–998.
[30] Lavalle, S.N., Hernandez, J., Mellon, P.L., 2020. OR16-01 the expression of the homeodomain transcription factor SIX3 within kisspeptin neurons is necessary for reproduction in mice. Journal of the Endocrine Society 4(Suppl 1). OR16-1.
[31] Liu, W., Lagutin, O.V., Mende, M., Streit, A., Oliver, G., 2006. Six3 activation of Pax6 expression is essential for mammalian lens induction and specification. The EMBO Journal 25(22):5383–5395.

[32] Cravo, R.M., Margatho, L.O., Osborne-Lawrence, S., Donato Jr., J., Atkin, S., Bookout, A.L., et al., 2011. Characterization of Kiss1 neurons using transgenic mouse models. Neuroscience 173:37—56.
[33] Atkinson, S.E., Maywood, E.S., Chesham, J.E., Wozny, C., Colwell, C.S., Hastings, M.H., et al., 2011. Cyclic AMP signaling control of action potential firing rate and molecular circadian pacemaking in the suprachiasmatic nucleus. Journal of Biological Rhythms 26(3):210—220.
[34] Hoffmann, H.M., 2018. Determination of reproductive competence by confirming pubertal onset and performing a fertility assay in mice and rats. Journal of Visualized Experiments 140:e58352.
[35] Hoffmann, H.M., Tamrazian, A., Xie, H., Perez-Millan, M.I., Kauffman, A.S., Mellon, P.L., 2014. Heterozygous deletion of ventral anterior homeobox (vax1) causes subfertility in mice. Endocrinology 155(10):4043—4053.
[36] Larder, R., Clark, D.D., Miller, N.L., Mellon, P.L., 2011. Hypothalamic dysregulation and infertility in mice lacking the homeodomain protein Six6. Journal of Neuroscience 31(2):426—438.
[37] Schoeller, E.L., Tonsfeldt, K.J., Sinkovich, M., Shi, R., Mellon, P.L., 2021. Growth hormone pulses and liver gene expression are differentially regulated by the circadian clock gene Bmal1. Endocrinology 162(4):bqab023.
[38] Livak, K.J., Schmittgen, T.D., 2001. Analysis of relative gene expression data using real-time quantitative PCR and the 2(-Delta Delta C(T)) Method. Methods 25(4):402—408.
[39] Sokolove, P.G., Bushell, W.N., 1978. The chi square periodogram: its utility for analysis of circadian rhythms. Journal of Theoretical Biology 72(1):131—160.
[40] Yoo, S.H., Yamazaki, S., Lowrey, P.L., Shimomura, K., Ko, C.H., Buhr, E.D., et al., 2004. PERIOD2::LUCIFERASE real-time reporting of circadian dynamics reveals persistent circadian oscillations in mouse peripheral tissues. Proceedings of the National Academy of Sciences of the United States of America 101(15):5339—5346.
[41] Shinozaki, A., Misawa, K., Ikeda, Y., Haraguchi, A., Kamagata, M., Tahara, Y., et al., 2017. Potent effects of flavonoid nobiletin on amplitude, period, and phase of the circadian clock rhythm in PER2::LUCIFERASE mouse embryonic fibroblasts. PLoS One 12(2):e0170904.
[42] Pandolfi, E.C., Hoffmann, H.M., Schoeller, E.L., Gorman, M.R., Mellon, P.L., 2018. Haploinsufficiency of SIX3 abolishes male reproductive behavior rhrough disrupted olfactory development, and impairs female fertility through disrupted GnRH neuron migration. Molecular Neurobiology 55(11):8709—8727.
[43] Hoffmann, H.M., Larder, R., Lee, J.S., Hu, R.J., Trang, C., Devries, B.M., et al., 2019. Differential CRE expression in Ihrh-cre and GnRH-cre alleles and the impact on fertility in otx2-flox mice. Neuroendocrinology 108(4):328—342.
[44] Hoffmann, H.M., Gong, P., Tamrazian, A., Mellon, P.L., 2018. Transcriptional interaction between cFOS and the homeodomain-binding transcription factor VAX1 on the GnRH promoter controls Gnrh1 expression levels in a GnRH neuron maturation specific manner. Molecular and Cellular Endocrinology 461: 143—154.
[45] Meijer, J.H., Robbers, Y., 2014. Wheel running in the wild. Proceedings of the Royal Society B: Biological Sciences 281, 1786.
[46] Novak, C.M., Burghardt, P.R., Levine, J.A., 2012. The use of a running wheel to measure activity in rodents: relationship to energy balance, general activity, and reward. Neuroscience & Biobehavioral Reviews 36(3):1001—1014.
[47] Mereness, A.L., Murphy, Z.C., Forrestel, A.C., Butler, S., Ko, C., Richards, J.S., et al., 2016. Conditional deletion of Bmal1 in ovarian theca cells disrupts ovulation in female mice. Endocrinology 157(2):913—927.
[48] Loh, D.H., Kuljis, D.A., Azuma, L., Wu, Y., Truong, D., Wang, H.B., et al., 2014. Disrupted reproduction, estrous cycle, and circadian rhythms in female mice deficient in vasoactive intestinal peptide. Journal of Biological Rhythms 29(5): 355—369.
[49] Lacombe, A., Lelievre, V., Roselli, C.E., Muller, J.M., Waschek, J.A., Vilain, E., 2007. Lack of vasoactive intestinal peptide reduces testosterone levels and reproductive aging in mouse testis. Journal of Endocrinology 194(1):153—160.
[50] Terpstra, A.H., 2001. Differences between humans and mice in efficacy of the body fat lowering effect of conjugated linoleic acid: role of metabolic rate. Journal of Nutrition 131(7):2067—2068.
[51] Bechtold, D.A., Brown, T.M., Luckman, S.M., Piggins, H.D., 2008. Metabolic rhythm abnormalities in mice lacking VIP-VPAC2 signaling. American Journal of Physiology - Regulatory, Integrative and Comparative Physiology 294(2): R344—R351.
[52] Sohn, J.W., 2015. Network of hypothalamic neurons that control appetite. BMB Rep 48(4):229—233.
[53] Yoshimura, M., Conway-Campbell, B., Ueta, Y., 2021. Arginine vasopressin: direct and indirect action on metabolism. Peptides 142:170555.
[54] Kim, E.R., Xu, Y., Cassidy, R.M., Lu, Y., Yang, Y., Tian, J., et al., 2020. Paraventricular hypothalamus mediates diurnal rhythm of metabolism. Nature Communications 11(1):3794.
[55] Brüning, J.C., Gautam, D., Burks, D.J., Gillette, J., Schubert, M., Orban, P.C., et al., 2000. Role of brain insulin receptor in control of body weight and reproduction. Science 289(5487):2122—2125.
[56] Elias, C.F., Purohit, D., 2013. Leptin signaling and circuits in puberty and fertility. Cellular and Molecular Life Sciences 70(5):841—862.
[57] Quennell, J.H., Mulligan, A.C., Tups, A., Liu, X., Phipps, S.J., Kemp, C.J., et al., 2009. Leptin indirectly regulates gonadotropin-releasing hormone neuronal function. Endocrinology 150(6):2805—2812.
[58] Egan, O.K., Inglis, M.A., Anderson, G.M., 2017. Leptin signaling in AgRP neurons modulates puberty onset and adult fertility in mice. Journal of Neuroscience 37(14):3875—3886.
[59] Low, M.J., Otero-Corchon, V., Parlow, A.F., Ramirez, J.L., Kumar, U., Patel, Y.C., et al., 2001. Somatostatin is required for masculinization of growth hormone-regulated hepatic gene expression but not of somatic growth. Journal of Clinical Investigation 107(12):1571—1580.
[60] Chowen-Breed, J.A., Steiner, R.A., Clifton, D.K., 1989. Sexual dimorphism and testosterone-dependent regulation of somatostatin gene expression in the periventricular nucleus of the rat brain. Endocrinology 125(1):357—362.
[61] Argente, J., Chowen-Breed, J.A., Steiner, R.A., Clifton, D.K., 1990. Somatostatin messenger RNA in hypothalamic neurons is increased by testosterone through activation of androgen receptors and not by aromatization to estradiol. Neuroendocrinology 52(4):342—349.
[62] Swindell, W.R., 2007. Gene expression profiling of long-lived dwarf mice: longevity-associated genes and relationships with diet, gender and aging. BMC Genomics 8(1):353.
[63] Romero, C.J., Pine-Twaddell, E., Sima, D.I., Miller, R.S., He, L., Wondisford, F., et al., 2012. Insulin-like growth factor 1 mediates negative feedback to somatotroph GH expression via POU1F1/CREB binding protein interactions. Molecular and Cellular Biology 32(21):4258—4269.
[64] Wallenius, K., Sjogren, K., Peng, X.D., Park, S., Wallenius, V., Liu, J.L., et al., 2001. Liver-derived IGF-I regulates GH secretion at the pituitary level in mice. Endocrinology 142(11):4762—4770.
[65] Kopchick, J.J., List, E.O., Kelder, B., Gosney, E.S., Berryman, D.E., 2014. Evaluation of growth hormone (GH) action in mice: discovery of GH receptor antagonists and clinical indications. Molecular and Cellular Endocrinology 386(1—2):34—45.
[66] Wauthier, V., Waxman, D.J., 2008. Sex-specific early growth hormone response genes in rat liver. Molecular Endocrinology 22(8):1962—1974.
[67] Luo, S., Zhang, Y., Ezrokhi, M., Li, Y., Tsai, T.H., Cincotta, A.H., 2018. Circadian peak dopaminergic activity response at the biological clock pacemaker (suprachiasmatic nucleus) area mediates the metabolic responsiveness to a high-fat diet. Journal of Neuroendocrinology 30(1):12563.
[68] Patton, D., Mistlberger, R., 2013. Circadian adaptations to meal timing: neuroendocrine mechanisms. Frontiers in Neuroscience 7:185.
[69] Parr, E.B., Heilbronn, L.K., Hawley, J.A., 2020. A time to eat and a time to exercise. Exercise and Sport Sciences Reviews 48(1):4—10.

[70] Hughes, A.T.L., Samuels, R.E., Bano-Otalora, B., Belle, M.D.C., Wegner, S., Guilding, C., et al., 2021. Timed daily exercise remodels circadian rhythms in mice. Commun Biol 4(1):761.

[71] Bebas, P., Goodall, C.P., Majewska, M., Neumann, A., Giebultowicz, J.M., Chappell, P.E., 2009. Circadian clock and output genes are rhythmically expressed in extratesticular ducts and accessory organs of mice. The FASEB Journal 23(2):523—533.

[72] Alvarez, J.D., Hansen, A., Ord, T., Bebas, P., Chappell, P.E., Giebultowicz, J.M., et al., 2008. The circadian clock protein BMAL1 is necessary for fertility and proper testosterone production in mice. Journal of Biological Rhythms 23(1): 26—36.

[73] Joye, D.A.M., Rohr, K.E., Keller, D., Inda, T., Telega, A., Pancholi, H., et al., 2020. Reduced VIP expression affects circadian clock function in VIP-IRES-CRE mice (JAX 010908). Journal of Biological Rhythms 35(4):340—352.

[74] Pandolfi, E.C., Breuer, J.A., Nguyen Huu, V.A., Talluri, T., Nguyen, D., Lee, J.S., et al., 2020. The homeodomain transcription factors Vax1 and Six6 are required for SCN development and function. Molecular Neurobiology 57(2): 1217—1232.

[75] Branda, C.S., Dymecki, S.M., 2004. Talking about a revolution: the impact of site-specific recombinases on genetic analyses in mice. Developmental Cell 6(1):7—28.

[76] Schmidt, E.E., Taylor, D.S., Prigge, J.R., Barnett, S., Capecchi, M.R., 2000. Illegitimate Cre-dependent chromosome rearrangements in transgenic mouse spermatids. Proceedings of the National Academy of Sciences of the U S A 97(25):13702—13707.

[77] Rempe, D., Vangeison, G., Hamilton, J., Li, Y., Jepson, M., Federoff, H.J., 2006. Synapsin I Cre transgene expression in male mice produces germline recombination in progeny. Genesis 44(1):44—49.

[78] Dubois, N.C., Hofmann, D., Kaloulis, K., Bishop, J.M., Trumpp, A., 2006. Nestin-Cre transgenic mouse line Nes-Cre1 mediates highly efficient Cre/loxP mediated recombination in the nervous system, kidney, and somite-derived tissues. Genesis 44(8):355—360.

[79] Ho, Y., Hu, P., Peel, M.T., Chen, S., Camara, P.G., Epstein, D.J., et al., 2020. Single-cell transcriptomic analysis of adult mouse pituitary reveals sexual dimorphism and physiologic demand-induced cellular plasticity. Protein Cell 11(8):565—583.

